



Zircon trace element geochemistry of the neoproterozoic late-granite suites along the southern margin of the Zimbabwe craton, Zimbabwe

Godfrey S. Chagondah^{a,*}, Marlina A. Elburg^a, Axel Hofmann^a, Hugh Rollinson^b, Henriette Ueckermann^a, Clarisa Vorster^a

^a Department of Geology, University of Johannesburg, Auckland Park, 2006, Johannesburg, South Africa

^b School of Built and Natural Environment, University of Derby, Kedleston Road, Derby DE22 1GB, UK

ARTICLE INFO

Handling Editor: M Mapeo

ABSTRACT

In-situ laser ablation quadrupole inductively coupled plasma mass spectrometry (LA-Q-ICP-MS) analyses of zircon grains from the ca. 2635–2620 Ma Chilimanzi and Razi granite suites along the southern margin of the Zimbabwe Craton in Zimbabwe reveal that a majority of zircons experienced post-magmatic chemical alteration. A minority (5 %) of the analyses show unaltered (*Type-1*) patterns. *Type-1* zircons show low abundances of light rare earth elements (LREE) relative to heavy rare earth elements (HREE) and they preserve igneous zoning textures. The majority of the grains analysed exhibit altered (*Type-2*) patterns indicated by overabundance in LREE concentrations and such grains are partially or completely metamict (radiation damaged). *Type-2* grains experienced radiation damage due to high initial contents of radioactive elements including U and Th incorporated at the time of crystallization. The structurally defective zircons experienced pervasive chemical alteration from *Type-1* to *Type-2* compositions via susceptible regions such as fractures under fluid-mediated conditions. Lack of analyses with $\text{Th/U} \leq 0.08$, which is a diagnostic feature of zircons precipitated from hydrothermal-melts supports the view that *Type-2* compositions derived from alteration of *Type-1* zircons. LREE overabundance in the zircon suites is also explained by inadvertent analysis of mineral inclusions and/or contaminants such as Fe, Ti, and Mn oxides along fractures.

Our study established a LREE index, $\text{LREE-I} = 32$ as a discriminant for altered and unaltered zircon analyses. $\text{LREE-I} < 32$ (altered compositions) correlates with known alteration features such as cathodoluminescence dark core domains, partial or complete overprint of igneous textures in fluid-mediated conditions, overabundance in LREE, and high contents of non-structural elements in zircon such as Ti, Li, Th and U. The Ti-in-zircon thermometry on unaltered analyses of the Chilimanzi Suite's Great Zimbabwe granite constrains the crystallization temperature at 698–738 °C, consistent with temperatures at zircon saturation for felsic magmas. Our study emphasizes that zircon chemistry is a pre-requisite data layer that should be incorporated in analytical protocols to complement conventional, discordance-based data filter for effective screening of U-Pb analyses for age determinations.

1. Introduction

The southern margin of the Zimbabwe Craton (ZC) comprises Meso- and Neoproterozoic greenstone belts (Fig. 1) that are in tectonic contact with a ca. 3.5–2.8 Ga tonalite-trondhjemite-granodiorite (TTG) suite (Taylor et al., 1991; Wilson et al., 1995; Hofmann and Chagondah, 2019; Hofmann et al., 2022). The greenstones and granitoids are intruded and surrounded by ca. 2635–2620 Ma syn- to late-tectonic potassic granites

of the Chilimanzi and Razi suites (Fig. 1; Mkweli et al., 1995; Frei et al., 1999; Horstwood et al., 1999; Chagondah et al., 2023). Globally, granites are characterized by diverse geochemical signatures that reflect variations in chemistry of the magma sources, geodynamic settings and petrogenetic processes (Barbarin, 1999; Robb et al., 2021; Rollinson, 2023).

Zircon (ZrSiO_4) is a ubiquitous accessory mineral in igneous, sedimentary and metamorphic rocks. Oscillatory zoning, also called growth

* Corresponding author.

E-mail addresses: geolochagondah@yahoo.com (G.S. Chagondah), marlinae@uj.ac.za (M.A. Elburg), ahofmann@uj.ac.za (A. Hofmann), h.rollinson@derby.ac.uk (H. Rollinson), henrietteu@uj.ac.za (H. Ueckermann), Clarisav@uj.ac.za (C. Vorster).

<https://doi.org/10.1016/j.jafrearsci.2025.105619>

Received 12 August 2024; Received in revised form 26 January 2025; Accepted 10 March 2025

Available online 29 March 2025

1464-343X/© 2025 The Authors. Published by Elsevier Ltd. This is an open access article under the CC BY-NC-ND license (<http://creativecommons.org/licenses/by-nc-nd/4.0/>).

zoning, is the predominant texture of magmatic zircon (Corfu et al., 2003; Hoskin and Schaltegger, 2003; Zhang et al., 2010; Bell et al., 2019). In igneous rocks, zircon can preserve a wealth of geochronological, isotopic, geochemical and petrogenetic information on the conditions of growth and composition of the melt from which it crystallized (Belousova et al., 2002, 2006; Hoskin and Schaltegger, 2003; Gardiner et al., 2017). Through coupled substitutions into the Zr lattice site, zircon is known to incorporate an assortment of incompatible trace elements (e.g., Y, Th, U, Ta, Nb, Hf and (in small amounts) Ti and rare earth elements (REE)) into its structure (Belousova et al., 2002, 2006; Hancher and Watson, 2003), which has resulted in it being widely used in geochemical studies including investigations on the evolution of Earth's crust (Hoskin and Schaltegger, 2003; Hoskin, 2005; Vervoort and Kemp, 2016; Andersen and Elburg, 2022). The Ti content of zircon is a proxy of the zircon crystallization temperature, as other minerals may crystallize at different temperatures, and is thus widely used as a petrological tool and geothermometer in granitic zircons (Watson et al., 2006; Ferry and Watson, 2007; Schiller and Finger, 2019).

Zircons commonly reveal a large variation in internal structure and chemical composition from sample to sample, from grain-to-grain within individual samples, and from site to site within individual crystals, a phenomenon attributed to heterogeneous distribution of trace elements and alteration (Bowring and Williams, 1999; Hoskin and Ireland, 2000; Wilde et al., 2001; Corfu et al., 2003; Hoskin and Schaltegger, 2003; Rayner et al., 2005; Fu et al., 2008; Claiborne et al., 2010). Studies on detrital and igneous zircons have demonstrated that disturbed oscillatory zoning in cathodoluminescence (CL) imaging, complex age spectra and non-magmatic $\delta^{18}\text{O}$ values indicate presence of altered compositions in zircon population (Cavosie et al., 2004, 2005, 2006; Bell et al., 2019; Andersen and Elburg, 2022). Altered zircons typically reveal LREE enrichment, also called LREE overabundance, which is a

widely observed feature, particularly in ancient terrestrial zircons (Peck et al., 2001; Wilde et al., 2001; Whitehouse and Kamber, 2002; Geisler et al., 2003b; Rayner et al., 2005; Bell et al., 2016; Bolhar et al., 2021; Andersen and Elburg, 2022). Chemical alteration in zircons is post-magmatic and is localized along lattice defects that easily allow ion exchange under fluid-mediated conditions (Cavosie et al., 2006; Bell et al., 2019). Occasionally, ingress of fluids into the zircon structure could also be through textural discontinuities (e.g., zoning) and interfaces between zircon and other mineral inclusions (Corfu et al., 2003).

Felsic rocks of the Northern Marginal Zone (NMZ) and adjacent areas of the ZC have elevated levels of radiogenic elements such as Th, U, and other elements including Rb and K (Berger et al., 1995; Berger and Rollinson, 1997; Kramers et al., 2001; Rollinson, 2023). Thus, high U + Th content in the zircons could potentially create conditions conducive to zircon alteration and enrichment in trace elements through interaction of fluids with metamict (radiation-damaged) regions of the zircon lattice (Whitehouse and Kamber, 2002; Corfu et al., 2003; Hoskin, 2005; Bell et al., 2016, 2019). Another potential source of LREE enrichment in zircon is caused by incorporation of sub-surface mineral inclusions and crack mineralization of Ti, Fe, P and Mn oxides that contaminate in-situ analyses due to accidental overlap (e.g., Geisler et al., 2003b; Cavosie et al., 2006; Bell et al., 2016, 2019; Pidgeon et al., 2019). Chemically altered zircons are unsuitable for isotopic analysis (Krogh, 1982; Andersen and Elburg, 2022).

In the last three decades, there has been much progress in in-situ analytical and imaging techniques with high spatial resolution, such as laser ablation quadrupole inductively coupled plasma mass spectrometry and CL, for the analysis of zircon. The in-situ techniques can minimise inadvertent analysis of crystal imperfections such as visible surface mineral inclusions (e.g., apatite, titanite, monazite, allanite) and

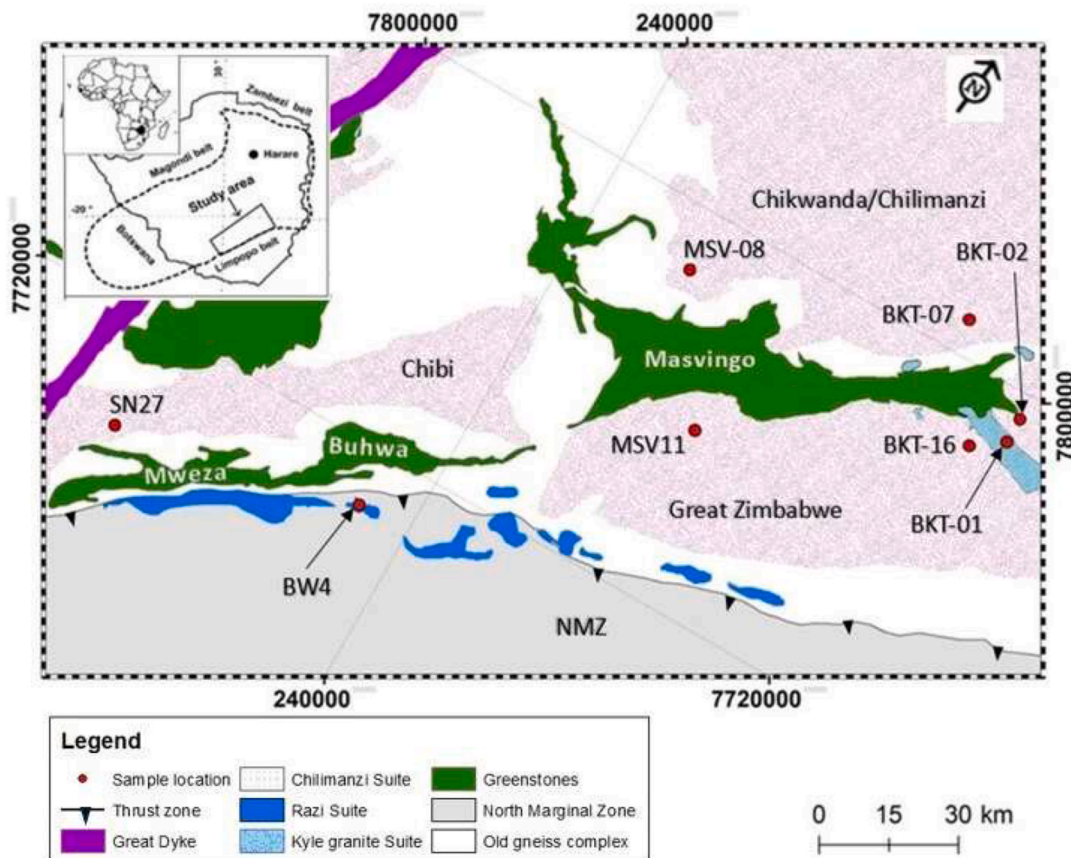


Fig. 1. Simplified geological map of the southern margin of the ZC (modified from Hofmann and Chagondah, 2019). Insert map shows the location of the study area and approximate boundaries of the ZC. Map units are UTM meters (zone 36 K) in WGS84 datum.

radiation-damaged domains that affect the analysis (Hoskin et al., 1998; Hoskin and Schaltegger, 2003). Despite this technological advancement, there has been no attempt to characterize zircon geochemistry of granitoids of the ZC and infer their geologic history. Trace element analysis is also increasingly becoming an important layer of information in resolving ambiguity in filtering isotopic data for age determinations (Hoskin and Schaltegger, 2003; Andersen and Elburg, 2022).

In this study, we use LA-Q-ICP-MS geochemical data to evaluate the integrity of zircon geochemistry as tracers of primary melt compositions and chemical alteration processes (e.g., Rayner et al., 2005; Hoskin, 2005; Andersen and Elburg, 2022). Our ultimate objective is to integrate the zircon chemical record with existing geochronological and whole-rock based models to characterize the geologic history of the granite suites along the southern margin of the ZC. We also employ Ti-in-zircon geothermometry on unaltered zircons to constrain crystallization temperatures of the magmas in the respective granite suites.

2. Geological setting

The southern part of the ZC is a Palaeo-to Mesoarchaean granitoid-greenstone terrain that is in tectonic contact with the NMZ of the Limpopo Belt that has been subjected to thrusting and high-grade metamorphism in the Neoarchaean (Fig. 1; Blenkinsop et al., 2004; Rollinson and Whitehouse, 2011; Hofmann and Chagondah, 2019). Metaluminous, I-type potassic granites of the ca. 2635–2620 Ma Chilimanzi and Razi suites intruded the area, prior to and concomitant with incipient thrusting of the NMZ (Fedo and Eriksson, 1996; Chagondah et al., 2023).

The Chilimanzi Suite consists of thick sub-horizontal sheets of granite, which were emplaced at shallow crustal levels throughout the ZC, with the magmatism accompanying its cratonization (Wilson et al., 1995; Jelsma et al., 1996; Blenkinsop and Treloar, 2001; Chagondah et al., 2023). Along the southern margin of the ZC it is represented by the oval-shaped Chibi, Chikwanda and Great Zimbabwe plutons (Fig. 1). The Kyle Granite of Robertson (1973) is part of the Chilimanzi Suite (Frei et al., 1999; Chagondah et al., 2023); it consists of a series of coarse-grained to porphyritic granodiorites-granites which are distributed within the ZC (Fig. 1). The boundary between the ZC and the NMZ is intruded by a series of porphyritic granodiorites of the Razi Suite. The suite formed through crustal anatexis accompanying thrusting of the NMZ onto the ZC (Mkweli et al., 1995; Blenkinsop et al., 1995).

Both suites formed by intracrustal melting of TTGs in the lower-middle crust, with no mantle contribution (Blenkinsop, 2011; Rollinson and Whitehouse, 2011; Rollinson, 2023; Chagondah et al., 2023). This proposition is given credence by evolved isotopic systems such as relatively high initial Sr isotopic ratios of 0.704–0.706, ϵ_{Nd} values, unradiogenic Hf isotopic signatures and the presence of xenoliths and inherited zircons in the younger granite suites (Hickman, 1978; Berger et al., 1995; Mkweli et al., 1995; Kramers et al., 2001; Rollinson and Whitehouse, 2011; Chagondah et al., 2023).

The NMZ is a granulite-facies terrain consisting of magmatic quartzofeldspathic gneisses (enderbites and charnockites) of the TTG-suite (Berger and Rollinson, 1997; Blenkinsop et al., 2004). The NMZ is regarded as a lower crustal section of the ZC entity (Mkweli et al., 1995; Rollinson and Blenkinsop, 1995; Rollinson and Whitehouse, 2011; Rollinson, 2023; Chagondah et al., 2024).

2.1. Mineralogy and petrography of the Razi and Chilimanzi suites

2.1.1. Razi Suite

The mineralogy and petrography of the Razi Suite is summarized from previous whole-rock studies by Chagondah (2022) and Chagondah et al. (2023). The Razi Suite exhibits two facies including the ubiquitous porphyritic variety and the fine-grained type that is hosted within the former. On outcrop scale, the porphyritic variety has aligned K-feldspar megacrysts of up to 30 mm. The alignment is a result of magma flow and

syn-tectonic emplacement. This study concentrates on the fine-grained facies of the Razi Suite, which occurs as a microgranite hosted within the porphyritic Razi Pluton. The Razi Suite comprises K-feldspar, plagioclase, quartz, biotite and minor hornblende and orthopyroxene. Accessory phases include magnetite, titanite, zircon, garnet, apatite, allanite, and rutile. Hydrothermal activity in the genesis of the microgranite is exhibited by presence of micro-quartz veins that truncate earlier formed grains (Chagondah et al., 2023). The Razi Suite plagioclase exhibits myrmekite and *anti*-perthite textures.

2.1.2. Chilimanzi Suite

The Chilimanzi Suite consists of light-grey, homogeneous and medium-to coarse-grained plutons. The mineralogy and petrography of the Chilimanzi granite is summarized from Chagondah et al. (2023). The suite comprises equigranular alkali feldspar, plagioclase, quartz, biotite, and muscovite. Magnetite, zircon, chlorite (after biotite), apatite, titanite, monazite and allanite constitute the accessory phases. The suite is characterized by higher degrees of metasomatic alteration (albitisation and sericitization) compared to the Razi Suite. Similarly, to the Razi Suite, plagioclase shows myrmekite and perthitic textures.

The Kyle Granite comprises coarse-grained to porphyritic granite. Alkali feldspar, quartz and plagioclase are the main mineral phases. Biotite and hornblende constitute minor phases. Accessory minerals include magnetite, titanite, zircon, apatite, garnet, allanite, and rutile.

3. Previous zircon U-Pb-Hf isotopic analysis

The Chilimanzi and Razi suite samples studied here were previously characterized for zircon U-Pb and Lu-Hf isotopic compositions by Chagondah et al. (2023). Locations, field photographs and descriptions of samples from which zircons were extracted is presented in Fig. 1, Supplementary Fig. S1 and Supplementary Table 1. CL imaging of zircons reveals a combination of preserved patterns, and partial to complete overprints on oscillatory and sector zoning patterns. All analyses reveal Th/U ratios >0.08 which affirms their magmatic origin (e.g., Hoskin and Ireland, 2000; Kramers and Mouri, 2011). However, a large number of grains are metamict, with CL-dark core and bright rim domains. The grains exhibit lattice defects indicated by fractured domains. Generally, zircon analysis document mostly discordant and few concordant (>90 % concordance) dates.

The studied zircon suites yielded a large spectrum of $^{207}\text{Pb}/^{206}\text{Pb}$ dates from 3206 to 2533 Ma, that represent inherited, magmatic and metamorphic ages. Lu-Hf analyses yielded unradiogenic compositions that reflect anatexis of pre-existing crustal protoliths (Chagondah et al., 2023). In this study, the grains were analysed with the consideration that some measured compositions could represent altered zircons.

4. Methods

4.1. Zircon LA-Q-ICP-MS trace element analysis and data reduction

In-situ LA-Q-ICP-MS was used for trace element measurements on zircon grains extracted from eight samples representing the Chilimanzi and Razi suites. Zircon grain mounts used in this study were previously prepared for U-Pb and Lu-Hf analyses by Chagondah (2022) and Chagondah et al. (2023) at the University of Johannesburg's Spectrum Analytical Facility (see Fig. 1 for sample locations). These zircons have not been previously characterized for mineral or melt inclusions.

The zircon chemical composition in this study was determined over four analytical sessions. Different regions in the same grains that resembled each other in CL were analysed for chemical composition (e.g. Fig. 2) and U-Pb and Lu-Hf isotopic compositions by Chagondah (2022) and Chagondah et al. (2023). Thus, the domains ablated in this study could be of different ages to the previously analysed sites. Apart from sample BKT-07 (Chikwanda Pluton) that had one grain analysed, an average of seven crystals, selected from grains that had given

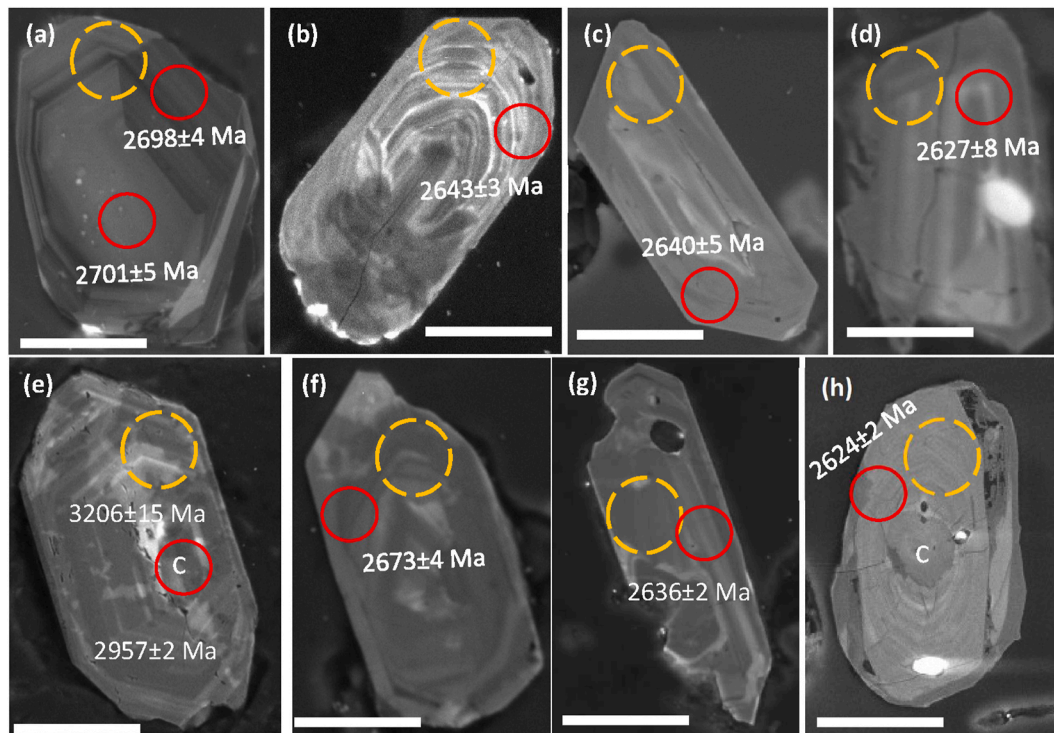


Fig. 2. CL images for representative zircon crystals from the Chilimanzi and Razi suites that were analysed for their geochemical composition using LA-ICP-MS. Analytical locations are such that 20 μm diameter red circles = $^{207}\text{Pb}/^{206}\text{Pb}$ ages and 30 μm diameter orange broken circles = trace element chemical compositions. C = inherited core. All scale bars are 50 μm . Fig. 2 (a) and (b) zircons gave the most typical type-1 pattern: (a) — Well-formed oscillatory zonation (BKT-02, gr63-1), (b) — Pronounced oscillatory zonation (BKT-16, gr50-1), (c) — Euhedral prism with obliterated zonation (MSV11, gr55-1), (d) — Cracked grain with growth zonation (BKT-01, gr20), (e) — Distinct oscillatory zonation enveloping a dark, inherited core (MSV-08, gr7), (f) — Partially preserved growth zonation (to centre) in a largely zonation obliterated prism (BKT-07, gr39), (g) — Growth zoning partially obliterated. Note cracking from dark ore domain (SN27, gr1), and (h) — Inherited dark core domain enveloped by distinct rim oscillatory zoning. Note radial fracturing away from core (BW4, gr17). Dates are from Chagondah (2022) and Chagondah et al. (2023).

concordant dates ranging from 3.21 to 2.53 Ga but dominated by ca. 2.63 Ga ages, were analysed per sample. Previously determined zircon U-Pb crystallization ages of the plutons from which zircon samples were extracted are given in Table 1 (Chagondah et al., 2023). A combination of CL reflected and transmitted light imaging were used prior to analysis to select flawless, unaltered, crack- and inclusion-free sites as much as possible. Typically, single spot analysis was done on regions showing seemingly unaltered magmatic zoning, as they are regarded to document zircon primary chemical compositions (e.g., Fu et al., 2008; Bell et al., 2016, 2019). As these were the same criteria used for selecting our U-Pb spots, it is likely that the trace element data match the U-Pb data acquired previously.

The LA-Q-ICP-MS analyses were done in-situ using a 193 nm ArF RESOLUTION SE excimer laser (Australian Scientific Instruments, Fyshwick) coupled to a Thermo Fisher iCAP RQ ICP-MS. The analytical operating conditions were as follows: RF Power 1550 W, coolant gas flow 14.0 L/min, auxiliary gas flow 0.80 L/min, nebuliser gas flow 0.98 L/min and laser He gas flow 0.35 L/min. Isotopes measured and dwell times (s) are: $^7\text{Li} = 0.05$, $^{31}\text{P} = 0.07$, $^{44}\text{Ca} = 0.01$, $^{49}\text{Ti} = 0.01$, $^{65}\text{Cu} = 0.04$, $^{71}\text{Ga} = 0.02$, $^{85}\text{Rb} = 0.03$, $^{89}\text{Y} = 0.01$, $^{90}\text{Zr} = 0.005$, $^{93}\text{Nb} = 0.02$, $^{139}\text{La} = 0.04$, $^{140}\text{Ce} = 0.01$, $^{141}\text{Pr} = 0.04$, $^{146}\text{Nd} = 0.02$, $^{147}\text{Sm} = 0.02$, $^{151}\text{Eu} = 0.04$, $^{153}\text{Eu} = 0.04$, $^{157}\text{Gd} = 0.02$, $^{159}\text{Tb} = 0.02$, $^{160}\text{Gd} = 0.02$, $^{163}\text{Dy} = 0.01$, $^{165}\text{Ho} = 0.01$, $^{167}\text{Er} = 0.01$, $^{169}\text{Tm} = 0.01$, $^{173}\text{Yb} = 0.01$, $^{175}\text{Lu} = 0.01$, $^{178}\text{Hf} = 0.005$, $^{181}\text{Ta} = 0.04$, $^{182}\text{W} = 0.04$, $^{205}\text{Tl} = 0.03$, $^{206}\text{Pb} = 0.005$, $^{207}\text{Pb} = 0.01$, $^{232}\text{Th} = 0.005$ and $^{238}\text{U} = 0.005$.

Trace element measurements were done on following conditions: 30 μm spot size, 7 Hz repetition rate, fluence of 4.0–4.2 J/cm^2 , 25 s acquisition of the gas blank signal and 70 s sample ablation. Previous U-Pb analysis utilized a 30 μm beam spot size.

NIST610 glass was used as a primary reference material for external

calibration, with reference values reported by Jochum et al. (2011). ^{90}Zr was used as internal standard, with an assumed concentration of 49 6007 ppm, which is the amount of zirconium in a stoichiometrically perfect zircon crystal. The error introduced by the presence of other elements (e.g., Hf) would not add significantly to the uncertainty inherent in LA-Q-ICPMS trace element analyses. GJ-1 (Piazolo et al., 2017), and USGS glass standard BCR-2G were used as secondary standards to evaluate accuracy. A bracketing approach was followed to correct for laser-induced elemental fractionation and mass bias, with analyses of standard reference materials conducted before and after every 10 batches of unknowns. In all analytical sessions, the laser ablation element analyses are such that zircon GJ-1 varies from 0.3 to 5 %, and the BCR-2G glass is between 0.75 and 1 % of analytical error of recommended values (Piazolo et al., 2017). All quality control data are included in Supplementary Table 2.

GLITTER (GEMCOC Laser ICPMS Total Element Reduction) 2008 v.4.5 software (Griffin et al., 2008) was employed for off-line data reduction. The software was used to inspect and evaluate the time resolved background and sample signal, drift calibrations and calculation of trace element concentration through its dynamic graphics and analysis tables. For background correction, contributions for each mass analysed prior to ablation was subtracted from sample signal.

4.2. Ti-in-zircon thermometry

Ti-in-zircon content is strongly dependent on temperature and activities of silica (a_{SiO_2}) and titanium (a_{TiO_2}) in the melt at the time of crystallization (Ferry and Watson, 2007; Schiller and Finger, 2019). Titanium concentration in zircon is an indicator of zircon minimum crystallization temperature (Watson and Harrison, 2005; Watson et al.,

2006). The Ti-in-zircon thermometer is used in systems containing rutile (Watson and Harrison, 2005). However, many silicic magmas are saturated in a Ti-bearing phases such as titanite, ilmenite and titaniferous magnetite, thus there is high apparent TiO_2 activity close to unity (Watson et al., 2006; Ferry and Watson, 2007). Although the Razi and Chilimanzi suites show rutile in places, titanite is a common accessory phase (Chagondah et al., 2023), which renders the application of Ti-in-zircon thermometry in determining crystallization temperatures of the granite suites. We used the model of Watson et al. (2006) to predict the crystallization temperatures for the studied granite suites:

$$T(^{\circ}\text{C})_{\text{zircon}} = \frac{5080 \pm 30}{(6.01 \pm 0.03) - \log(\text{Ti})} - 273$$

where T is temperature in degrees Celsius, Ti is element's concentration in ppm, and the uncertainties are 2σ .

Schiller and Finger (2019) observed that granitic melts display subunity $a\text{SiO}_2$ ranging from 0.9 to 1.0. Granites are typically emplaced at depths of 1–30 km (ca. 0.1–1.0 GPa) at crystallization temperatures of 690–880 °C (Scaillet and MacDonal, 2001; Storm and Spear, 2005; Schiller and Finger, 2019), which is consistent with natural zircons crystallization at upper crustal pressures (0.7–3 GPa) and temperature (580–1070 °C) calibration used in Ti-in-zircon thermometer by Watson et al. (2006). The Ti-in-zircon thermometer calibration shows little sensitivity to pressure effect over the range of conditions relevant to the Earth's crust (e.g., Ryerson and Watson, 1987; Watson and Harrison, 2005; Watson et al., 2006). Assessment of the Ti-in-zircon thermometry was based on unaltered magmatic compositions of zircons from the various samples.

5. Results

5.1. Zircon morphology and internal structures

Morphologies and internal structures of representative zircon crystals are presented in CL images (Fig. 2; Supplementary Figs. S2–S8). The grains reveal a wide range of variation in size, internal textures and CL characteristics. The zircons are generally homogeneous prisms that exhibit a wide range of sizes up to 170 μm in length. The crystals reveal complex internal structures such as well-preserved to weak oscillatory zoning bands, superimposed sector zoning, resorption features and radial or irregular cracks. The growth zoning patterns in the studied granite suites resemble those from other igneous zircon textures such as in the Boggy Plain aplite, south-eastern Australia (Hoskin and Schaltegger, 2003; Hoskin, 2005; Ickert et al., 2011). The Boggy Plain aplite is well-documented for hosting unaltered crustal magmatic zircons with typical unaltered REE patterns (Hoskin, 2005). Furthermore, similarly to the studied granites, the intrusion is an I-type granite. A number of grains are altered, as indicated by partial preservation to complete overprint of growth zoning textures (Fig. 2b, c, f & g; Supplementary Figs. S2–S8). In places, evidence of uncharacterized mineral and/or melt inclusions are revealed as bright, un-zoned sectors within oscillatory zoning regions (Fig. 2a–d, g & h; Supplementary Figs. S2d & e, S4e, S5a & d, S6a & c, S7a & b and S8c).

Some of the grains display inherited dark core domains devoid of CL zoning surrounded by oscillatory brighter rims (Fig. 2c and h; Supplementary Figs. S2c, S3b–c, S4c, S5a & c, S6a & b and S8c). Based on Chagondah et al. (2023), some of the CL-dark core domains in zircons are variably metamict between different growth zones. Similar studies in the Boggy Plain aplite observed that CL-dark zones are characterized by U and Th enrichment (Ickert et al., 2011). A large number of crystals show fracturing (Fig. 2b–d & h).

5.2. Geochemistry of the zircons

Zircon trace element concentrations of representative samples from

the Chilimanzi and Razi suites are presented in Table 1. Three grains from the Great Zimbabwe Pluton including BKT-02 gr6-1, BKT gr63-1 and BKT-16 gr50-1 show lower concentrations of 0.02, 0.07 and 1.42 ppm La compared to 3.7–502 ppm La in rest of the analyses (Table 1; Fig. 2).

See attached excel file.

Note: Light rare earth element index ($\text{LREE-I} = \text{Dy/Sm} + \text{Dy/Nd}$) (using concentrations rather than chondrite-normalized values) (Bell et al., 2016, 2019). $\text{Ce/Ce}^* = \text{Ce}_{\text{CN}}/(\text{La}_{\text{CN}} * \text{Pr}_{\text{CN}})^{0.5}$ and $\text{Eu/Eu}^* = \text{Eu}_{\text{CN}}/(\text{Sm}_{\text{CN}} * \text{Gd}_{\text{CN}})^{0.5}$ (Trail et al., 2012). CN = Chondrite-normalized.

5.2.1. Trace element variations

Zircons in the studied granite suites reveal a wide range in REE, Li, Ti, U and Th abundances (Table 1). Ti abundances span a 6–14242 ppm range, with 17 % of zircons exhibiting high (>25 ppm) Ti values. In other studies, it is observed that zircon with primary igneous compositions typically reveal <25 ppm Ti (e.g., Hoskin, 2005; Watson and Harrison, 2005; Fu et al., 2008; Schiller and Finger, 2019). The Chilimanzi and Razi suite zircon show U and Th contents of 79–4820 and 81–3545 ppm, respectively. Li versus U + Th contents show a positive correlation (Fig. 3).

5.2.2. Chondrite-normalized diagrams

Chondrite-normalized diagrams for zircons from the two granite suites (Fig. 4) reveal REE patterns depicting Type-1 (unaltered) and Type-2 (altered) compositions (e.g., Hoskin, 2005; Cavosie et al., 2006). In order to visualize and evaluate the difference between unaltered and altered zircons, our REE data is plotted alongside igneous zircon population data from the Boggy Plain aplite which shows typical Type-1 REE patterns of magmatic zircon (Hoskin, 2005).

The Boggy Plain aplite REE pattern is characterized by a steep increase in normalized concentration from La to Lu, with occurrence of distinct positive Ce and negative Eu anomalies (Fig. 4), that are typical signatures of magmatic zircons derived from crustal igneous rocks (e.g., Hinton and Upton, 1991; Belousova et al., 2002; Hoskin and Schaltegger, 2003; Hoskin and Ireland, 2000; Bell et al., 2019). The LREE are depleted relative to heavy rare earth elements (HREE) concentration. Among the studied granites, only three zircon analysis (BKT-02 gr6-1, BKT-02 gr63-1 and BKT-16 gr50-1) from the Great Zimbabwe granite show (Type-1) REE patterns that are similar or overlap with zircon from the Boggy Plain aplite (Fig. 4a and b).

The majority of the analysed zircon samples from both granite suites are altered and show Type-2 patterns (Fig. 4c–h). Type-2 analyses display flat, high abundance of LREEs ranging from 10s to 100s times chondritic values, with weak to absent Ce and Eu anomalies compared to Type-1 patterns. Type-2 analyses exhibit low $(\text{Sm/La})_{\text{CN}}$ values, ranging from 0.6 to 7.2, avg. = 2.1 vs. 57–119 for magmatic zircon (e.g., Hoskin et al., 2000) and weak Ce (Ce/Ce^*) of 1.2–6.8, avg. = 2.7 vs. 39–40 for magmatic zircon (e.g., Hoskin et al., 2000) and slightly high Eu (Eu/Eu^*) of 0.2–0.9, avg. = 0.4 vs. 0.2–0.3 for magmatic zircon (e.g., Hoskin et al., 2000) anomalies (Fig. 4; Table 1). Similar Type-2 patterns are reported in terrestrial zircons by Hoskin (2005) and Cavosie et al. (2006). The HREE abundances define a slight concave-down curvature and are in some cases lower than Type-1 abundances. Type-2 analysis show lower average $(\text{Lu/Gd})_{\text{CN}}$ value of 12, with nearly 80 % of the analyses revealing an average of 8 vs 16 for Type-1 analyses.

5.2.3. Ti-in-zircon thermometry

Among the studied granites, Ti-in-zircon thermometry was only evaluated for three analyses from the Chilimanzi Suite's Great Zimbabwe Pluton (samples BKT-02 and BKT-16) that represent unaltered (Type-1) magmatic zircon compositions (Fig. 4a and b). The Great Zimbabwe Pluton is quartz saturated and contains titanite (Chagondah et al., 2023) which suggests relatively high activities of $a\text{SiO}_2$ and $a\text{TiO}_2$ (e.g., Claiborne et al., 2010; Ickert et al., 2011). Ti-in-zircon

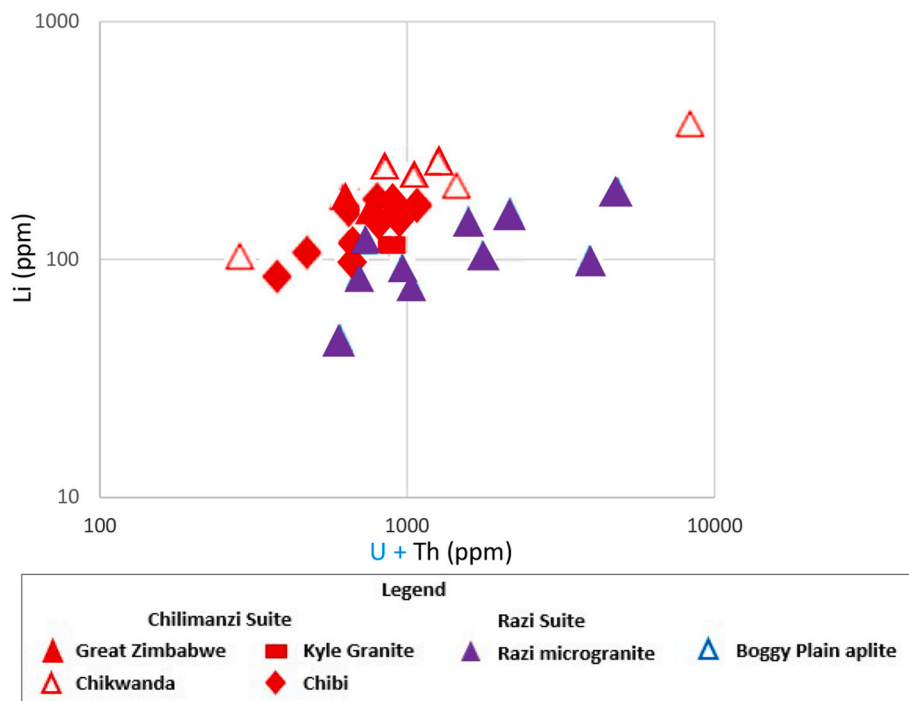


Fig. 3. Li versus U + Th diagram for samples from the Chilimanzi and Razi suites. Magmatic zircon samples from the Boggy Plain aplite after Hoskin (2005) are plotted for comparison.

temperatures were estimated using Watson et al. (2006) model. The Great Zimbabwe Pluton magmatic zircons, with 6.0–9.7 ppm Ti (Table 1) reveal crystallization temperatures of between 698 and 738 °C.

6. Discussion

6.1. Magma source for the parental granite suites

CL imaging of zircons reveal complex internal structures such as inherited CL-dark cores overgrown by bright rims and metamict zircons (Fig. 2c and h; Supplementary Figs. S2c, S3b-c, S4c, S5a & c, S6a & b and S8c) that indicate that parental magmas for both granite suites assimilated pre-existing rocks during magma ascent or that partial melting of the source was incomplete (e.g., Hofmann et al., 2020; Robb et al., 2021; Rowe et al., 2022). Multi-population U-Pb age data coupled with xenocrystic relationships confirm the structural complexity of these zircons (Chagondah, 2022; Chagondah et al., 2023).

6.2. Zircon chemical compositions

Cavosie et al. (2006) emphasized in their study of Jack Hills zircons that Type-1 (unaltered) and Type-2 (altered) categories (see Fig. 4) refer to REE patterns in analysed spots within a grain domain, and not necessarily across the entire grain. The authors observed that at least one zircon crystal from their study exhibits both types of patterns. Similar observations are corroborated in studies of zircons from a granitic dyke from the Acasta Gneiss Complex, Canada (e.g., Bowring and Williams, 1999; Corfu et al., 2003; Rayner et al., 2005) who used back-scattered electron microscopy and reflected light microscopy images to recognize altered and unaltered domains with contrasting REE patterns within a single grain.

Despite our effort to focus trace element spot analyses on zircon in regions with seemingly magmatic zoning textures, flawless and inclusion free domains (Fig. 2: Supplementary Figs. S2–S8), the results yielded only three unaltered compositions and a majority of chemically altered compositions (Fig. 4). This is not surprising, as the work by Chagondah et al. (2023) also yielded predominantly discordant U-Pb

dates for the same zircons. However, even altered and discordant zircons are still likely to provide reliable Hf isotope data, provided the Lu/Hf ratios remain low (Andersen and Elburg, 2022). High-LREE in zircons may be a result of multiple factors, including localized fluid-assisted alteration of radiation damaged parts of grains and inadvertent analysis of crack mineralization and hidden mineral inclusions (e.g., Whitehouse and Kamber, 2002; Hoskin and Schaltegger, 2003; Hoskin, 2005; Bell et al., 2016). In the following sections, we evaluate the potential causes of alteration in zircons from the studied granite suites.

6.2.1. Chemical alteration of zircons under fluid-flow

Previous characterization of the zircons from the Razi and Chilimanzi suites for U-Pb isotopic compositions reveal that more than 84 % of the analyses are discordant and this is pronounced in grains with dark core and fractured rim domains (Chagondah, 2022; Chagondah et al., 2023). Similar observations are made in this study that despite some grains showing growth zoning textures, crystals with CL-dark core and brighter rim zones likely experienced radiation damage and became metamict (Fig. 2c and h; Supplementary Figs. S2c, S3b-c, S3c, S5a & c, S6a & b and S8c). Metamict crystals suffer structural lattice damage from the decay of radiogenic elements (U and Th incorporated at the time of crystallization), typically develop amorphous domains and metamictization-induced fractures (e.g., Pidgeon et al., 1966; Ordóñez et al., 1989; Whitehouse and Kamber, 2002; Corfu et al., 2003; Bell et al., 2015). Fluid-alteration leads to partial or complete resetting of the zircon age record due to disturbance of the U-Pb system (Mezger and Krogstad, 1997). During interaction with aqueous fluids, metamict zircon commonly loses radiogenic Pb causing normal U-Pb discordance (Pidgeon et al., 2019; Andersen and Elburg, 2022). Textureless zircons Supplementary Figs. S3, S4b-c, S5b-c, S6, & S8c) are interpreted to have experienced overprint by aqueous fluids. The presence of remnant oscillatory zoning in altered zircon supports the view that Type-2 analyses represent altered Type-1 compositions.

Partially metamict or metamict grains have lattice defects that are susceptible to chemical alteration through ingress of aqueous fluids (Belousova et al., 2002; Geisler et al., 2003b; Bell et al., 2016, 2019; Andersen and Elburg, 2022). There is a positive correlation between Li

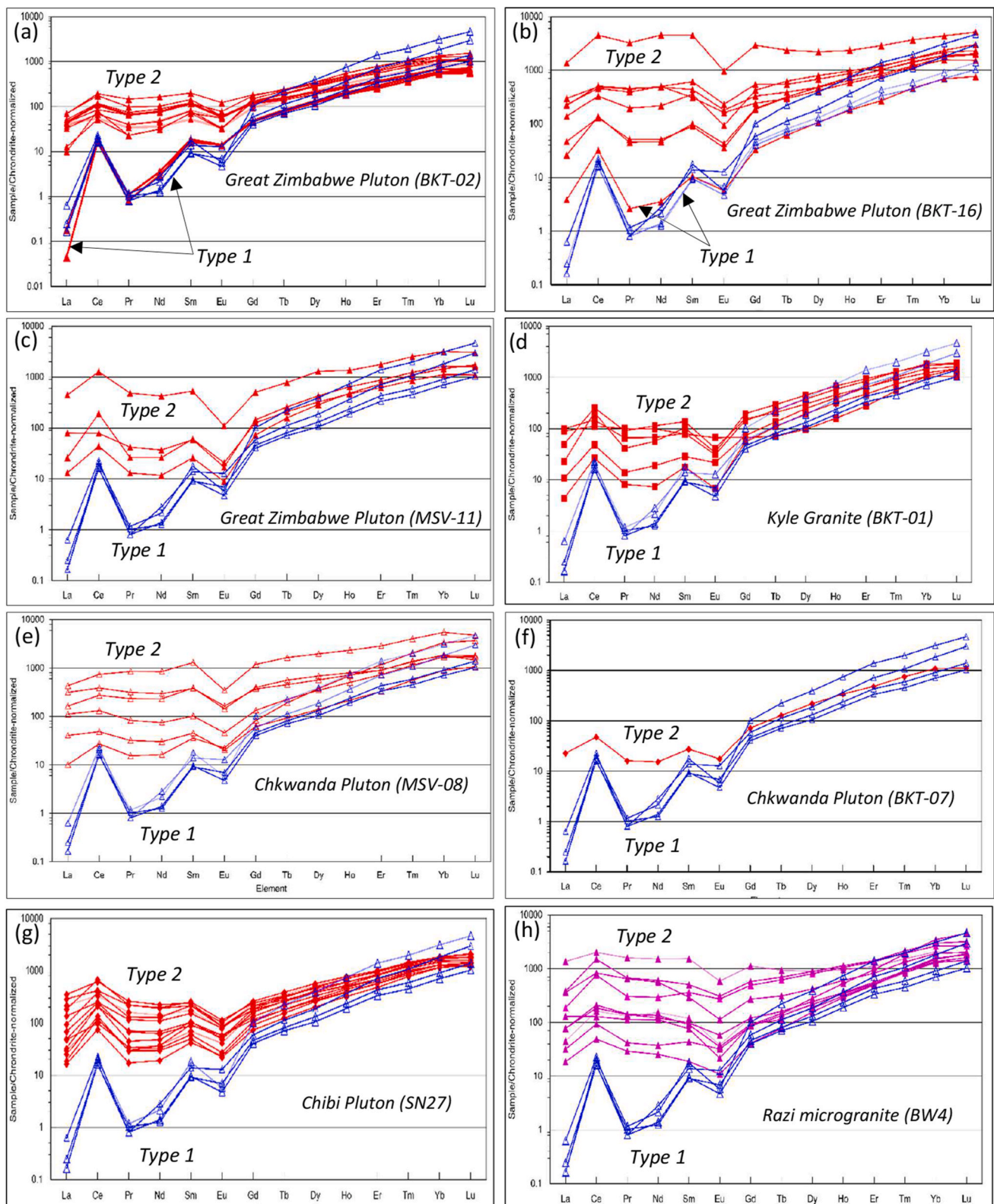


Fig. 4. Chondrite-normalized REE profiles for the zircon samples and suites. Great Zimbabwe Pluton samples: (a) — BKT-02, (b) — BKT-16 & (c) — MSV11, (d) — Kyle granite (BKT01), (e) — Chikwanda Pluton (MSV08), & (f) — Chikwanda Pluton (BKT-07), (g) — Chibi Pluton (SN27), and (h) — Razi microgranite (BW4). Boggy Plain aplite (BP42) after Hoskin (2005) (blue open triangles) is given for comparison for magmatic zircon REE patterns. Chilimanzi Suite samples are in open and filled red symbols, and Razi Suite microgranite is in pink filled triangle. Normalization data from Taylor and McLennan (1985). This study used LA-Q-ICP-MS analysis, whereas Boggy Plain aplite data were analysed using SIMS technique. LA-Q-ICP-MS and SIMS analyses yield comparable data in terms of accuracy and precision (~5–15 %) for trace-element analysis of zircon (Hoskin, 1998; Hoskin et al., 2000). Symbols as shown in Fig. 3.

vs U + Th contents (Fig. 3), with high U and Th abundances causing metamictization of zircon and allowing incorporation of elements that are normally incompatible in the zircon lattice. This causes preferential incorporation of REE and non-structural elements such as Li, Ti, Mn and Fe-oxides during subsequent geological events (Whitehouse and Kamber, 2002; Corfu et al., 2003; Cavosie et al., 2006; Bell et al., 2016). Ti-, Mn- or Fe-oxides or hydroxides could be precipitated along cracks (Cavosie et al., 2006; Pidgeon et al., 2019). Loss of HREE (Fig. 4c–h) and other heavy trace elements relative to magmatic zircons has been documented in other studies (e.g., Geisler et al., 2003a; Hoskin and Schaltegger, 2003). Whitehouse and Kamber (2002) proposed that if LREE enrichment in zircon (Fig. 4c–h) is a result of radiation damage of the crystal lattice, a correlation is expected in the U + Th vs La_{CN} plot. Indeed, our data shows a positive correlation ($R^2 = 0.60$) (Fig. 5) across both granite suites and supports the proposition that LREE enrichment in the studied granite zircons is attributed to metamictization. Our study suggests a $La_{CN} < 4$ value as a discriminant for unaltered and altered magmatic zircon compositions (Table 1; Fig. 5).

In summary, this study shows that zircons with high LREE concentrations are correlated with structural markers of alteration features shown in CL images such as metamict regions, fractures, remnant magmatic zoning and partial to complete fluid overprint of oscillatory zoning (Table 1; Fig. 2; Supplementary Figs. S2–S8). Furthermore, altered analysis has high contents of non-formula elements such as Ti, U, and Th (Table 1; Fig. 5).

Hoskin (2005) proposed fields to discriminate zircons of magmatic and hydrothermal origin using La vs. chondrite normalized Sm/La diagram (Fig. 6). Our zircon data show that only two grains plot within the magmatic field whereas a majority of the analyses either plot inside or near the hydrothermal field (Fig. 6). A number of analyses are intermediate between magmatic and hydrothermal zircons. Unlike the hydrothermal zircon described by Hoskin (2005), which has blurred zones or porous structures, altered zircons from this study exhibit preserved oscillatory zones typical of magmatic zircons. Thus, we interpret that Type-2 analysis are products of chemical alteration of Type-1 zircons under fluid-mediated conditions.

6.2.2. Inadvertent analysis

Zircon, titanite, allanite, apatite and monazite are some of the main reservoirs of LREE (Bea, 1996; Smithies et al., 2018; Rollinson and Pease, 2021). Although due care was taken to select flawless and inclusion free grain domains using CL, reflected and transmitted light

imaging, it is possible that some analyses incorporated hidden mineral inclusions and crack mineralization into the analysed volume, with the signal spreading over the entire analysis (e.g., Hoskin et al., 2000; Whitehouse and Kamber, 2002; Geisler et al., 2003a; Cavosie et al., 2006; Zhang et al., 2010; Bell et al., 2019). Unintentional analysis is inherent to the LA-Q-ICP-MS technique because it ablates a larger volume compared to SIMS. The analysed grains show more cracks compared to inclusions (Fig. 2; Supplementary Figs. S2–S8). Mineralization along cracks causes incorporation of exotic materials such as Fe, Ti, and Mn oxides (e.g., Corfu et al., 2003; Watson et al., 2006; Bell et al., 2015; 2016; Pidgeon et al., 2019) and potential adsorption of LREE to the oxides. Thus, even zircon with seemingly magmatic oscillatory zoning could have yielded Type-2 abundances after analyses of sub-surface LREE-bearing mineral inclusions and crack mineralization during sampling (Figs. 2 and 4c–h; Supplementary Figs. S2 to S8).

Whitehouse and Kamber (2002) proposed that exotic elements (e.g., Th, U, P, Ti) vs $(La/Sm)_{CN}$ diagram may be used to investigate a correlation and thus establish if overabundance in the exotic materials is due to contaminants or otherwise. There is no correlation both in the P and Ti vs $(La/Sm)_{CN}$ plots (Fig. 7a and b) suggesting that the overabundance in the exotic elements is not caused by analysis of contaminants such as P and Ti oxides along structurally defective zircons. The plots also test for unintentional analysis of P-bearing minerals (e.g., monazite & apatite) and Ti-bearing phases (e.g., titanite, ilmenite or titaniferous magnetite). In Fig. 7b, the analyses with the highest Ti do not have the highest chondrite normalized Sm/La. That would more likely suggest a role for a mineral that contains Ti but no LREE.

6.3. Quantitative criteria for recognizing altered analyses using LREE-based alteration index

In zircon analyses, abundances of LREE are a good alteration indicator (Hoskin, 2005; Hoskin and Schaltegger, 2003; Cavosie et al., 2006; Andersen and Elburg, 2022). Other qualitative discriminants for altered zircons includes $Ce > 50$ ppm (Hoskin and Schaltegger, 2003), $(Sm/La)_{CN}$ ratio of 1.5–4.4 (Hoskin, 2005) and $La_{CN} > 10$ (Zhang et al., 2010) and $Pr_{CN} > 10$ (Cavosie et al., 2006). Cavosie et al. (2006) pointed out that the $La_{CN} > 1$ and $Pr_{CN} > 10$ for Type-2 (altered zircons) composition is generally intermediate between magmatic and hydrothermal fields of Hoskin (2005). In most cases, qualitative discrimination of unaltered and altered samples is ambiguous. Bell et al. (2016, 2019) proposed a quantitative criterion for discriminating altered and unaltered zircon compositions. The authors suggested the light rare earth element index ($LREE-I = Dy/Sm + Dy/Nd$) (using concentrations rather than chondrite-normalized values). According to these authors, the LREE-I tracks the changes in LREE pattern due to either interaction with hydrothermal fluid or contamination of zircon by exotic materials such as Ti-, Fe- and Mn-oxides. In a study of Jack Hills detrital zircons, Bell et al. (2016) suggested that $LREE-I < 30$ represent altered zircon compositions, whereas pristine (unaltered) magmatic zircon compositions show $LREE-I > 30$. With the uncertainty if the $LREE-I > 30$ values derived from detrital zircon are representative of magmatic zircon compositions worldwide, Bell et al. (2019) analysed granitic suites with ages of 15–730 Ma from the USA and defined an even higher $LREE-I > 60$ for magmatic compositions.

Our data reveal that a LREE-I vs. Ti and Ce/Ce* diagrams indicate a break in slope at LREE-I value of about 32 and $Ce/Ce^* \geq 10$ suggesting that this could be the value that discriminates unaltered and altered zircons (Fig. 8). The $LREE-I = 32$ cutoff value in this study is in agreement with $LREE-I = 30$ of Bell et al. (2016) on their Palaeoarchean-Hadean zircons. This similarity suggests similar magma composition or contaminants and hydrothermal fluids effecting alteration conditions unlike in the Neoproterozoic-Phanerozoic granitoid zircons which yielded higher LREE-I value of 60 (Bell et al., 2019). $LREE-I = 32$ corresponds to maximum concentrations of ca. 300 ppm U and 9.7 ppm Ti, with inferred Ti-in-zircon crystallization temperature of

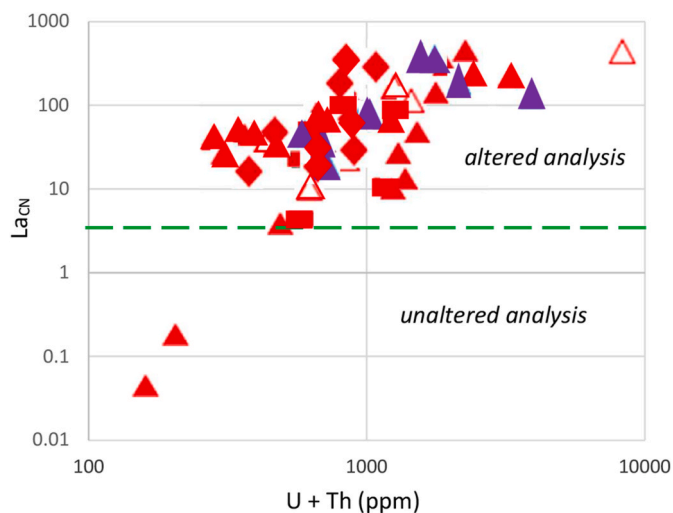


Fig. 5. U + Th vs La_{CN} diagram showing discrimination of altered and unaltered zircon analysis at a cut-off value of $La_{CN} = 4$ which is consistent with low (≤ 1.42 ppm) La contents shown in Table 1. Dotted horizontal line represents $La_{CN} = 4$. Symbols as shown in Fig. 3.

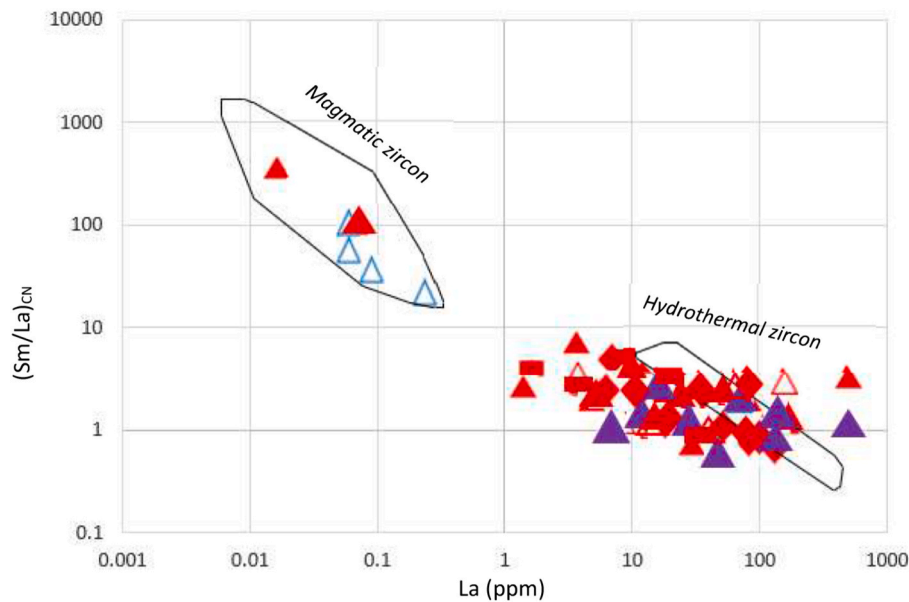


Fig. 6. Magmatic and hydrothermal zircon discrimination plots for the Chilimanzi and Razi suite zircons using chondrite-normalized Sm/La ratio vs. La (ppm) (fields after Hoskin, 2005). Magmatic zircon data (open triangles) from Boggy Plain aplite are plotted for comparison. Symbols as shown in Fig. 3.

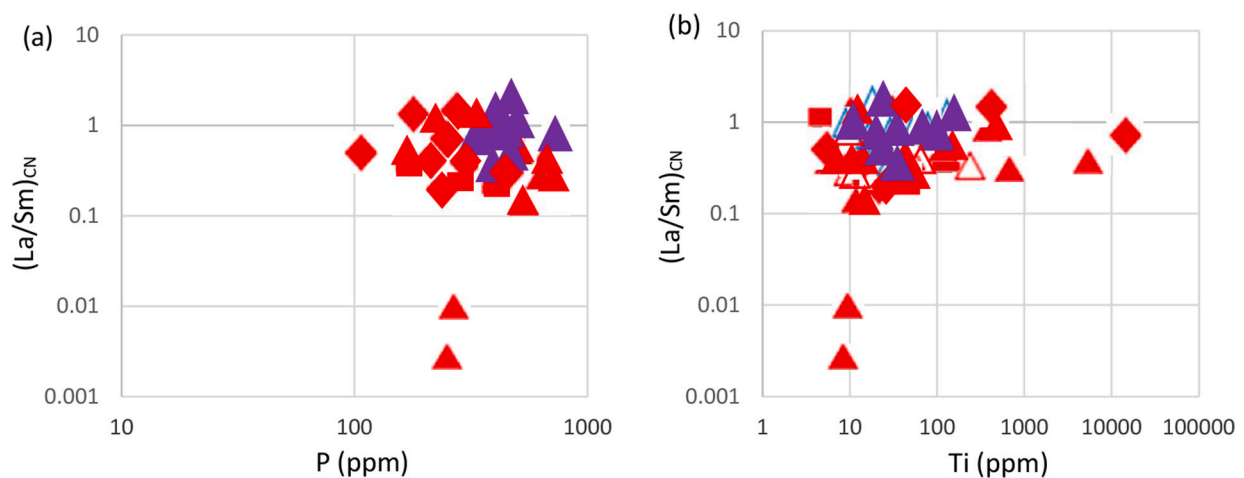


Fig. 7. Degree of LREE enrichment (expressed as $(La/Sm)_{CN}$) versus geochemical indicators of possible contamination by exotic materials in the zircon analysis. (a) — P vs $(La/Sm)_{CN}$ and (b) — Ti vs $(La/Sm)_{CN}$. P and Ti are used to test for the presence of P-bearing minerals (e.g., monazite & apatite) and Ti-bearing phases (e.g., titanite, ilmenite or titaniferous magnetite) respectively. Symbols as shown in Fig. 3.

ca. 698–738 °C. *Type-2* grains with $LREE-I < 32$ are associated with known indicators of alteration and contamination in zircon such as disturbance to oscillatory zoning, low Ce/Ce^* , high-LREE, U, Th, Ti, and common Pb abundances (Fig. 4c–h, 7 & 9).

The $LREE-I > 32$ value is in agreement with chondrite-normalized plots (Fig. 4a and b) which show that only three grains from the Great Zimbabwe granite have igneous, *Type-1* REE patterns. Other alteration indicators including moderate magnitude Ce/Ce^* value of 4.5, $Pr_{CN} < 10$ (e.g., Cavosie et al., 2006), $La_{CN} < 10$ (e.g., Zhang et al., 2010) and reasonable magmatic concentration values of ≤ 16 ppm Ti (e.g., Fu et al., 2008; Schiller and Finger, 2019) (Table 1) support this proposition. Therefore, based on $LREE-I$, Ce/Ce^* , Pr_{CN} and La_{CN} values, it is likely that one of the zircons from the Kyle Granite is only slightly altered.

6.4. Th/U ratio as a discriminant of magmatic and metamorphic-melt zircons

Apart from few crystals exhibiting partial to complete overprint of

igneous textures, the majority of studied zircons are characterized by euhedral to subhedral morphologies, with well-preserved to weak oscillatory zoning which suggests magmatic origin (Fig. 2; Supplementary Figs. S2–S8; Hoskin and Schaltegger, 2003). However, this study reveals that a large proportion of such grains are altered (Fig. 4c–h, 7, 8, 9 & 10). Th/U ratio is widely used as a first order discriminant between zircons of igneous and metamorphic-melt origin (e.g., Hoskin and Ireland, 2000; Hoskin and Schaltegger, 2003). Typical Th/U ratio of magmatic zircon is between 0.4 and 1 (Hoskin and Ireland, 2000), whereas zircon originated from metamorphic-melt have a $Th/U \leq 0.08$ –0.01 (Rubatto, 2002; Kramers and Mouri, 2011).

Our data displays Th/U ratios of 0.14–2.57 (Fig. 9; Table 1) which indicates that all grains are magmatic. Hoskin (2005) pointed out that oscillatory and sector zoning reflect heterogeneous trace elements distribution in zircon, and this may explain variations in Th/U ratio (0.7–1.0) in unaltered zircon domains of the Great Zimbabwe Pluton. There is a conspicuous absence of zircons with $Th/U \leq 0.08$ which implies the absence of metamorphic crystals (e.g., Rubatto, 2002).

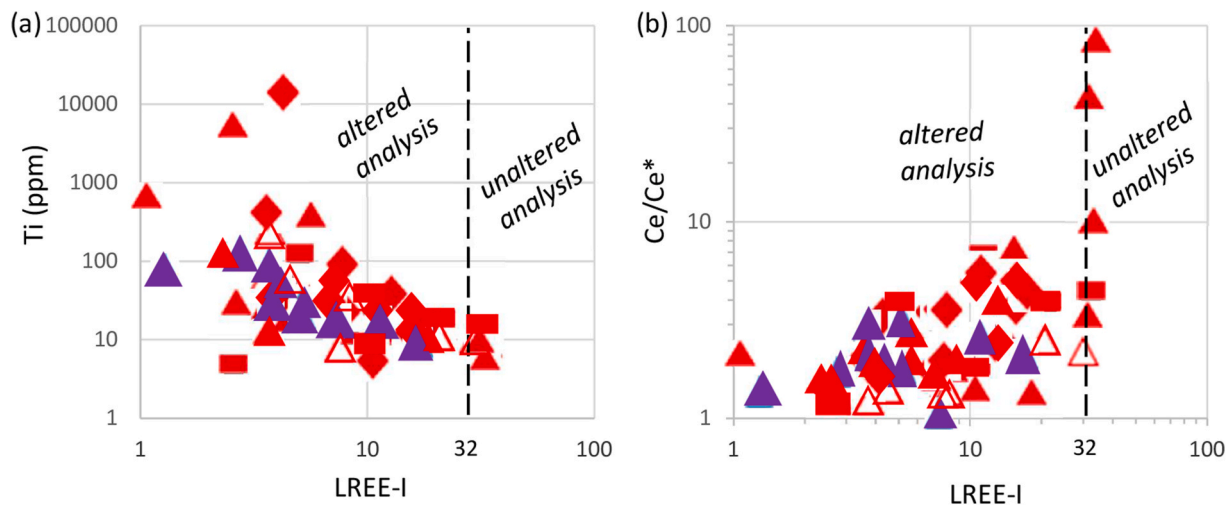


Fig. 8. (A) — LREE-I vs. Ti and (b) — LREE-I vs. Ce/Ce*. Vertical broken line represents LREE-I cutoff value of 32, with assumed unaltered analysis being >32 . LREE-I = $Dy/Sm + Dy/Nd$ (using concentrations rather than chondrite-normalized values). Symbols as shown in Fig. 3.

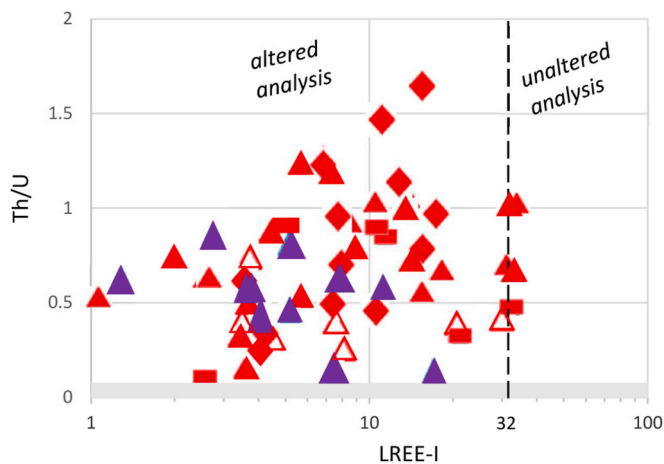


Fig. 9. Variation of Th/U versus LREE-I. The shaded area represents field for zircons derived from metamorphic melt with $Th/U \leq 0.08$ (Rubatto, 2002; Kramers and Mouri, 2011). Vertical broken line depicts LREE-I cutoff value of 32, with unaltered analysis represented by LREE-I > 32 . LREE-I = $Dy/Sm + Dy/Nd$ (using concentrations rather than chondrite-normalized values). Symbols as shown in Fig. 3.

Instead, the altered zircons experienced fluid-assisted alteration from *Type-1* to *Type-2* compositions as suggested in other studies (e.g., Hoskin and Schaltegger, 2003; Cavosie et al., 2006; Bell et al., 2016, 2019). High Th/U of >1.0 shown in some altered zircon, indicates more introduction of Th relative to U into radiation-damaged zircons (e.g., Pidgeon et al., 2019; Andersen and Elburg, 2022).

6.5. Inversion modelling of the unaltered zircons

We used the compositions of the unaltered zircons from the Great Zimbabwe Pluton and partition coefficient data from Sano et al. (2002) and Chapman et al. (2016) to calculate the REE composition of the melt (s) from which the zircons crystallized. These are illustrated on a chondrite-normalized REE plot in Fig. 10, relative to values in the whole rock samples. There are some differences in the results between the two different sets of partition coefficient data, notably for Eu and the middle REE, although the overall similarity between measured and calculated compositions validates this approach. It is assumed that since zircon is an early-crystallising phase in a granitic melt, the melt compositions

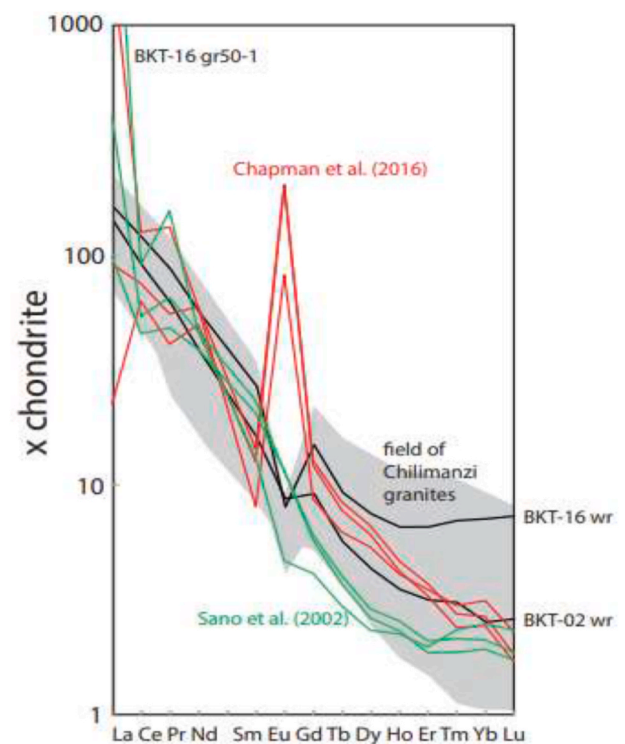


Fig. 10. Chondrite normalized melt compositions for REE in the Great Zimbabwe Pluton at the time of zircon crystallization calculated from the composition of unaltered zircons using the partition coefficient data of Sano et al. (2002) – green lines and Chapman et al. (2016) – red lines. The results are compared with REE in the measured whole-rock compositions (black lines designated BKT-16 wr and BKT-02 wr) and with the full range of compositions found in the Chilimanzi granite suite (grey field). Abbreviation: wr = whole rock. Whole-rock data for samples BKT-16, BKT-02 and entire Chilimanzi Suite is after Chagondah et al. (2023).

calculated here represent the composition of the parental melt, prior to any fractional crystallisation, whereas the composition of the whole-rock reflects the composition of the evolved melt after any fractional crystallisation. For this reason, it is worth investigating the small differences between the measured and calculated melt compositions. First however it is important to recognize that the discrepancies in the

light REE La, Ce and Pr may in part be due to the effects of alteration noted in other zircon grains, particularly for La in BKT-16 gr 50–1. The difference between measured and calculated concentrations for Eu are thought to be real (although the partition coefficient quoted by Chapman et al. (2016) may be in error) and reflect feldspar fractionation, most probably K-feldspar, which took place during the cooling of the melt and gave rise to the negative Eu-anomaly in the whole-rock samples. In addition, since the middle to heavy REE are highly incompatible in both plagioclase and K-feldspar it is likely that feldspar fractionation would also drive melt concentrations to higher values for the middle and heavy REE as observed.

6.6. Crystallization temperature of the granite suites

To predict a reliable crystallization temperature, the geological meaning of Ti concentrations in zircon should be understood. Granitic zircons typically contain <25 ppm Ti (Watson and Harrison, 2005; Harley and Kelly, 2007; Fu et al., 2008). Unreasonably high Ti values have limited geological meaning as they are associated with chemical alteration signatures or contaminants and are thus not used in Ti-in-zircon thermometry (e.g., Hoskin, 2005; Zhang et al., 2010).

Ti-in-zircon thermometer of Watson et al. (2006), predicts a narrow crystallization temperature range from 698 to 738 °C for the three magmatic zircons from the ca. 2629 Ma Great Zimbabwe Pluton that show 6.0–9.7 ppm Ti (Table 1; Fig. 4a and b). Whole-rock compositions in the Great Zimbabwe Pluton samples BKT-02 and BKT-16 which contain unaltered analyses reveal TiO₂ content of 0.20 wt % (Chagondah et al., 2023). Following the model of Hanchar and Watson (2003), this corresponds to Ti saturation temperatures of 771 °C, consistent with the range of Ti-in-zircon temperatures. Both the Ti-in-zircon and whole-rock Ti saturation temperatures are within 690–880 °C range of zircon saturation for felsic magmas in granitic systems (e.g., Schiller and Finger, 2019).

Experimental data from the Qz-Ab-Or-An system and phase equilibrium modelling by Rollinson et al. (2024) show that melts for the Chilimanzi Suite formed at ≥ 900 °C. Our upper range value of ca. 738 °C for the Ti-in-zircon crystallization temperature is consistent with minimum anatexis temperature of 900 °C suggested by Rollinson et al. (2024).

6.7. Implications for zircon geochronology

Previous characterization of the Chilimanzi and Razi suite samples for zircon U-Pb and Lu-Hf isotopic compositions showed that a majority of concordant or semi-concordant U-Pb dates were not used for determination of igneous crystallization ages for the granite suites (Chagondah, 2022; Chagondah et al., 2023). The excluded analyses reflect inherited ages from known magmatic events and younger metamorphic overprint age groups. Younger metamorphic age clusters of ca. 2600–2533 Ma are characterized by high contents of U, Th, and common Pb (Chagondah et al., 2023). Thus, only a few analyses from the zircon U-Pb and Lu-Hf isotopic compositions study were available for determination of crystallization ages, based on qualitative filtering of analyses based on U, Th, and common Pb concentrations. Our study shows that only three analyses from the Great Zimbabwe granite preserve magmatic compositions and show ≤300 ppm U and ≤200 ppm Th (Fig. 4a and b; Table 1). These values could provide maximum concentration, that may be useful data filters for screening analyses for U-Pb geochronology. It is likely that zircon U-Pb ages of 2517 ± 55 Ma and 2540 ± 38 Ma reported by Frei et al. (1999) for the Razi Suite's Mavizhu Pluton and Kyle Granite's Rezhura Pluton, respectively, represent altered analyses. Thus, the pervasive nature of the alteration brings into question some previous U-Pb analyses on zircon from granitoids along the southern margin of the Zimbabwe Craton.

Zircon trace element chemistry is useful in discriminating unaltered (*Type-1*) and altered (*Type-2*) spot analyses and should be included in

analytical protocols to complement conventional, discordance-based data filter for better screening of U-Pb analyses for age determinations, although this causes a major reduction in useful grains in the dataset. The altered analyses in this study may conflict with concordant or semi-concordant status from previous U-Pb and Lu-Hf analyses (Table 1; Chagondah, 2022; Chagondah et al., 2023), of same grains, but it is emphasized that the analyses were on different spots. This phenomenon of a single grain displaying both altered and unaltered compositions is observed and explained in other studies (e.g., Corfu et al., 2003; Rayner et al., 2005; Cavosie et al., 2006). We recommend that the trace element analyses are done concurrently with the U-Pb analyses, either by using split stream, or by using LA-Q-ICP-MS to measure trace and U-Pb at the same time. In this study, we note that fluid-assisted ion-exchange and thermal overprint resulted in chemical alteration and disturbance to the U-Pb isotope system (e.g., Mezger and Krogstad, 1997; Geisler et al., 2003a), with only 5 % out of 61 analyses retaining primary compositions. Altered analyses have limited geological meaning.

7. Conclusions

Whilst a majority of the studied zircons are variably chemically altered as attested by their *Type-2* REE patterns, a few grains preserve igneous zoning textures that are a diagnostic feature of primary magmatic zircon, and they show *Type-1* patterns. The absence of zircon analyses showing Th/U ≤ 0.08, in the studied zircon suites, suggests that zircons with *Type-2* patterns did not precipitate from hydrothermal melts, but instead reflect chemical alteration of *Type-1* compositions. Fluid-mediated chemical alteration by aqueous fluids was localized and channelled through susceptible regions such as fractures and metamict (radiation-damaged) zircons that had an initially high content of Th and U incorporated at the time of crystallization. In some grains, there was partial or complete metamorphic overprint of primary igneous textures by ingress of fluids. LREE enrichment in the zircon suites is also attributed to inadvertent analysis of sub-surface mineral inclusions and/or contaminants such as Ti, Fe and Mn oxides along fractures.

This study established an LREE-I cutoff value of 32 as a discriminant for altered and unaltered zircon analysis. LREE-I < 32 (altered compositions) correlates with known alteration features such as partial or complete overprint of magmatic textures, enrichment in LREE, Ti, U and Th. Thus, the LREE-I is a useful data filter as it removes the majority of chemically altered zircon. The turnover value of 32 is in agreement with a value of 30 published in literature. The Ti concentrations in magmatic zircon from the Great Zimbabwe granite constrain the crystallization temperature of the Chilimanzi Suite at between 698 and 738 °C, which is within range of zircon saturation for felsic magmas in granitic systems. Our study demonstrates that zircon chemistry is a pre-requisite data layer that must be included in analytical protocols to complement conventional, discordance-based data filter for effective screening of U-Pb analyses for age determinations, although this results in a major reduction in useful grains in the dataset.

Funding

Funding was sourced from the South African Department of Science and Innovation and was disbursed through the Centre of Excellence for Integrated Mineral and Energy Resource Analysis (DSI-NRF CIMERA).

CRedit authorship contribution statement

Godfrey S. Chagondah: Writing – original draft, Visualization, Validation, Investigation, Conceptualization. **Marlina A. Elburg:** Writing – review & editing, Visualization, Validation, Software, Methodology, Investigation, Data curation. **Axel Hofmann:** Writing – review & editing, Visualization, Supervision, Resources, Funding acquisition. **Hugh Rollinson:** Writing – review & editing, Validation, Formal

analysis. **Henriette Ueckermann:** Software, Methodology, Investigation, Formal analysis, Data curation. **Clarisa Vorster:** Writing – review & editing, Visualization, Validation.

Declaration of competing interest

The authors declare that they have no known competing financial interests or personal relationships that could have appeared to influence the work reported in this paper.

Acknowledgements

Godfrey S. Chagondah is grateful to the generous PhD bursary support from the South African Department of Science and Innovation disbursed through the Centre of Excellence for Integrated Mineral and Energy Resource Analysis (DSI-NRF CIMERA). Godfrey also acknowledges the financial support from the Society of Economic Geologists which was used for financing part of the analytical work. The University of Johannesburg LA-Q-ICP-MS equipment used for zircon geochemistry was funded by an NRF-NEP grant (No. 93208) and is supported by DSI-NRF CIMERA and the PPM (Paleoproterozoic Mineralization) research centre. Elizabeth A. Bell and an anonymous reviewer are thanked for their attentive reviews which improved clarity of the manuscript. Read B.M Mapeo is thanked for editorial handling.

Appendix A. Supplementary data

Supplementary data to this article can be found online at <https://doi.org/10.1016/j.jafrearsci.2025.105619>.

Data availability

Data will be made available on request.

References

- Andersen, T., Elburg, M.A., 2022. Open-system behaviour of detrital zircon during weathering: an example from the Palaeoproterozoic Pretoria Group, South Africa. *Geol. Mag.* 159, 561–576.
- Barbarin, B., 1999. A review of the relationships between granitoid types, their origins, and their geodynamic environments. *Lithos* 46, 605–626.
- Bea, F., 1996. Residence of REE, Y, Th and U in granites and crustal protoliths; implications for the chemistry of crustal melts. *J. Petrol.* 37, 521–552.
- Belousova, E.A., Griffin, W.L., O'Reilly, S.Y., Fisher, N.I., 2002. Igneous zircon: trace element composition as an indicator of source rock type. *Contrib. Mineral. Petrol.* 143, 602–622.
- Belousova, E.A., Griffin, W.L., O'Reilly, S.Y., 2006. Zircon crystal morphology, trace element signatures and Hf-isotope composition as a tool for petrogenetic modelling: examples from eastern Australian granitoids. *J. Petrol.* 7, 329–353.
- Bell, E.A., Boehnke, P., Barboni, M., Harrison, T.M., 2019. Tracking chemical alteration in magmatic zircon using rare earth element abundances. *Chem. Geol.* 510, 56–71.
- Bell, E.A., Boehnke, P., Harrison, T.M., 2016. Recovering the primary geochemistry of Jack Hills zircons through quantitative estimates of chemical alteration. *Geochem. Cosmochim. Acta* 191, 187–202.
- Bell, E.A., Boehnke, P., Hopkins-Wielicki, M.D., Harrison, T.M., 2015. Distinguishing primary and secondary inclusion assemblages in Jack Hills zircons. *Lithos* 234, 15–26.
- Berger, M., Kramers, J.D., Nägler, T.F., 1995. Geochemistry and geochronology of charnoenderbites in the northern marginal zone of the Limpopo Belt, Southern Africa, and genetic models. *Schweizerische Mineralogische und Petrographische Mitteilungen* 75, 17–42.
- Berger, M., Rollinson, H., 1997. Isotopic and geochemical evidence for crust-mantle interaction during late Archaean crustal growth. *Geochem. Cosmochim. Acta* 61, 4809–4829.
- Blenkinsop, T.G., 2011. Archaean magmatic granulites, diapirism, and proterozoic reworking in the northern marginal zone of the Limpopo belt. In: van Reenen, D.D., Kramers, J.D., McCourt, S., Perchuk, L.L. (Eds.), *Origin and Evolution of Precambrian High-Grade Gneiss Terranes*, with Special Emphasis on the Limpopo Complex of Southern Africa, vol. 207. Geological Society of America. Memoir, pp. 1–24.
- Blenkinsop, T.G., Kröner, A., Chiwara, V., 2004. Single stage, late Archaean exhumation of granulites in the Northern Marginal Zone, Limpopo Belt, Zimbabwe, and relevance to gold mineralization at Renco mine. *S. Afr. J. Geol.* 107, 377–396.
- Blenkinsop, T.G., Mkweli, S., Rollinson, H.R., Fedo, C.M., Paya, B.K., Kamber, B., Kramers, J., Berger, M., 1995. The North Limpopo thrust zone: the Northern boundary of the Limpopo belt in Zimbabwe and Botswana. In: Barton, J.R., Copperthwaite, Y.E. (Eds.), *Centennial Geocongress, Volume II: Johannesburg*, Geological Society of South Africa, pp. 174–177.
- Blenkinsop, T.G., Treloar, P.J., 2001. Tabular intrusion and folding of the late Archaean Murehwa granite, Zimbabwe during regional shortening. *J. Geol. Soc.* 158, 653–664. London.
- Bolhar, R., Hofmann, A., Allen, C.M., Maas, R., 2021. A LA-ICPMS zircon record of magmatic crystallization and compositional alteration in metaigneous rocks of the eastern Kaapvaal Craton. *S. Afr. J. Geol.* 123, 1–22.
- Bowring, S.A., Williams, I.S., 1999. Priscoan (4.00–4.03 Ga) orthogneisses from northwestern Canada. *Contrib. Mineral. Petrol.* 134, 3–16.
- Cavosie, A.J., Valley, J.W., Wilde, S.A., E, I.M.F., 2006. Correlated microanalysis of zircon: trace element, d18O, and U–Th–Pb isotopic constraints on the igneous origin of complex >3900 Ma detrital grains. *Geochem. Cosmochim. Acta* 70, 5601–5616.
- Chagondah, G.S., 2022. *Petrogenesis and Metallogenesis of Granitic Rare-Metal Pegmatites along the Southern Margin of the Zimbabwe Craton: Implications to Exploration* (Doctoral Thesis) Johannesburg. University of Johannesburg.
- Chagondah, G.S., Hofmann, A., Elburg, M.A., Iaccheri, L.M., Kramers, J.D., Wilson, A.H., 2023. Petrogenesis of potassic granite suites along the southern margin of the Zimbabwe Craton. *S. Afr. J. Geol.* 126, 1–28.
- Chagondah, G.S., Kramers, J.D., Hofmann, A., Rollinson, H., 2024. Neoproterozoic and Palaeoproterozoic tectono-metamorphic events along the southern margin of the Zimbabwe craton: insights from muscovite ⁴⁰Ar/³⁹Ar geochronology from rare-metal pegmatites, Zimbabwe. *J. Afr. Earth Sci.* 217, 105333.
- Chapman, J.B., Gehrels, G.E., Ducea, M.N., Giesler, N., Pullen, A., 2016. A new method for estimating parent rock trace element concentrations from zircon. *Chem. Geol.* 439, 59–70.
- Claiborne, L.L., Miller, C.F., Wooden, J.L., 2010. Trace element composition of igneous zircon: a thermal and compositional record of the accumulation and evolution of a large silicic batholith, Spirit Mountain, Nevada. *Contrib. Mineral. Petrol.* 160, 511–531.
- Corfu, F., Hanchar, J.M., Hoskin, P.O., Kinny, P., 2003. Atlas of zircon textures. *Rev. Mineral. Geochem.* 53 (1), 469–500.
- Fedo, C.M., Eriksson, K.A., 1996. Stratigraphic framework of the ~ 3.0 Ga buhwa greenstone belt: a unique stable-shelf succession in the Zimbabwe archaean craton. *Precamb. Res.* 77 (3), 161–178.
- Ferry, J.M., Watson, E.B., 2007. New thermodynamic models and revised calibrations for the Ti-in-zircon and Zr-in-rutile thermometers. *Contrib. Mineral. Petrol.* 154, 429–437.
- Frei, R., Schoenberg, R., Blenkinsop, T.G., 1999. Geochronology of the late archaean Razi and Chilimanzi suites of granites in Zimbabwe; implications for the late archaean tectonics of the Limpopo belt and Zimbabwe craton. *S. Afr. J. Geol.* 102, 55–63.
- Fu, B., Page, F., Cavosie, A., Fournelle, J., Kita, N., Lackey, J., Wilde, S., Valley, J., 2008. Ti-in-zircon thermometry: applications and limitations. *Contrib. Mineral. Petrol.* 156, 197–215.
- Gardiner, N.J., Hickman, A.H., Kirkland, C.L., Lu, Y.J., Johnson, T.E., Zhao, J.X., 2017. Processes of crust formation in the early earth imaged through Hf isotopes from the East Pilbara Terrane. *Precamb. Res.* 297, 56–76.
- Geisler, T., Pidgeon, R.T., Kurtz, R., Bronswijk, W.V., Schleicher, H., 2003a. Experimental hydrothermal alteration of partially metamict zircon. *Am. Mineral.* 88, 1496–1513.
- Geisler, T., Rashwan, A.A., Rahn, M.K.W., Poller, U., Zwingmann, H., Pidgeon, R.T., Schleicher, H., Tomaschek, F., 2003b. Low-temperature hydrothermal alteration of natural metamict zircons from the Eastern Desert, Egypt. *Mineral. Mag.* 67, 485–508.
- Griffin, W.L., Powell, W.J., Pearson, N.J., O'Reilly, S.Y., 2008. GLITTER: data reduction software for laser ablation ICP-MS. In: Sylvester, P. (Ed.), *Laser Ablation ICP-MS in the Earth Sciences: Current Practices and Outstanding Issues*, vol. 40. Mineralogical Association of Canada, Short Course Series, pp. 307–311.
- Hanchar, J.M., Watson, E.B., 2003. Zircon saturation thermometry. In: Hanchar, J.M., Hoskin, P.W.O. (Eds.), *Zircon. Reviews in Mineralogy and Geochemistry*, vol. 53, pp. 89–112.
- Harley, S.L., Kelly, N.M., 2007. The impact of zircon–garnet REE distribution data on the interpretation of zircon U–Pb ages in complex high-grade terranes: an example from the Rauer Islands, East Antarctica. *Chem. Geol.* 241, 62–87.
- Hickman, M.H., 1978. Isotopic evidence for crustal reworking of the rhodesian archaean craton, southern Africa. *Geology* 6, 214–216.
- Hinton, R.W., Upton, B.G.J., 1991. The chemistry of zircon - variations within and between large crystals from syenite and alkali basalt xenoliths. *Geochem. Cosmochim. Acta* 55, 3287–3302.
- Hofmann, A., Chagondah, G., 2019. The palaeoarchaean record of the Zimbabwe craton. In: Van Kranendonk, M., C, V., Bennett, V.C., Hoffmann, J.E. (Eds.), *Earth's Oldest Rocks*, second ed. Elsevier, Amsterdam, pp. 855–864.
- Hofmann, A., Kröner, A., Iaccheri, L.M., Wong, J., Geng, H., Xie, H., 2022. 3.63 Ga grey gneisses reveal the Eoarchaean history of the Zimbabwe craton. *S. Afr. J. Geol.* 125, 1–12. <https://doi.org/10.25131/sajg.125.0005>.
- Hofmann, A., Xie, H., Saha, L., Reinke, C., 2020. Granitoids and greenstones of the white mfolozi inlier, south-east kaapvaal craton. *S. Afr. J. Geol.* 123, 263–276.
- Horstwood, M.S.A., Nesbitt, R.W., Noble, S.R., Wilson, J.F., 1999. U–Pb zircon evidence for an extensive early Archaean craton in Zimbabwe: a reassessment of the timing of craton formation, stabilization, and growth. *Geology* 27, 707–710.
- Hoskin, P.W.O., 2005. Trace-element composition of hydrothermal zircon and the alteration of Hadean zircon from the Jack Hills, Australia. *Geochem. Cosmochim. Acta* 69, 637–648.
- Hoskin, P.W.O., 1998. Minor and trace element analysis of natural zircon (ZrSiO₄) by SIMS and laser ablation ICP-MS: a consideration and comparison of two broadly competitive techniques. *J. Trace Microprobe Tech.* 16, 301–326.

- Hoskin, P.W.O., Kinny, P.D., Wyborn, D., 1998. Chemistry of hydrothermal zircon: investigating timing and nature of water-rock interaction. In: Arehart, G.B., Hurlston, J.R. (Eds.), *Water-Rock Interaction, WRI-9*. AA Balkema, Rotterdam, pp. 545–548.
- Hoskin, P.W.O., Kinny, P.D., Wyborn, D., Chappell, B.W., 2000. Identifying accessory mineral saturation during differentiation in granitoid magmas: an integrated approach. *J. Petrol.* 41, 1365–1396.
- Hoskin, P.W.O., Schaltegger, U., 2003. The composition of zircon and igneous and metamorphic petrogenesis. *Rev. Mineral. Geochem.* 53, 27–62.
- Hoskin, P.W.O., Ireland, T.R., 2000. Rare earth element chemistry of zircon and its use as a provenance indicator. *Geology* 28, 627–630.
- Ickert, R., Williams, I., Wyborn, D., 2011. Ti in zircon from the Bogy Plain zoned pluton: implications for zircon petrology and Hadean tectonics. *Contrib. Mineral. Petrol.* 162, 447–461.
- Jelsma, H.A., Vinyu, M.L., Valbracht, P.J., Davies, G.R., Wijbrans, J.R., Verdurmen, E.A. T., 1996. Constraints on Archaean evolution of the Zimbabwe craton: a U-Pb zircon, Sm-Nd and Pb-Pb whole-rock isotope study. *Contrib. Mineral. Petrol.* 124 (1), 55–70.
- Jochum, K.P., Weis, U., Stoll, B., Kuzmin, D., Yang, Q., Raczek, I., Jacob, D.E., Stracke, A., Birbaum, K., Frick, D.A., Günther, D., Enzweiler, J., 2011. Determination of reference values for NIST SRM 610–617 glasses following ISO guidelines. *Geostand. Geoanal. Res.* 35, 397–429.
- Kramers, J.D., Mouri, H., 2011. The geochronology of the Limpopo Complex: a controversy solved. In: van Reenen, D.D., Kramers, J.D., McCourt, S., Perchuk, L.L. (Eds.), *Origin and Evolution of Precambrian High-Grade Gneiss Terranes, with Special Emphasis on the Limpopo Complex of Southern Africa*, vol. 207. Geological Society of America Memoir, pp. 85–106.
- Kramers, J.D., Kreissig, K., Jones, M.Q.W., 2001. Crustal heat production and style of metamorphism: a comparison between Archaean high grade provinces in the Limpopo Belt, southern Africa. *Precamb. Res.* 112, 149–163.
- Krogh, T.E., 1982. Improved accuracy of U-Pb zircon ages by the creation of more concordant systems using an air abrasion technique. *Geochem. Cosmochim. Acta* 46, 637–649.
- Mezger, K., Krogstad, E.J., 1997. Interpretation of discordant U-Pb zircon ages: an evaluation. *J. Metamorph. Geol.* 15, 127–140.
- Mkweli, S., Kamber, B., Berger, M., 1995. Westward continuation of the craton-Limpopo belt tectonic break in Zimbabwe and new age constraints on the timing of the thrusting. *J. Geol. Soc.* 152, 77–83. London.
- Ordóñez, R.E., Schleifer, J.J., Adloff, J.P., Roessler, K., 1989. Chemical effects of α -decay in uranium minerals. *Radiochim. Acta* 47, 177–185.
- Peck, W.H., Valley, J.W., Wilde, S.A., Graham, C.M., 2001. Oxygen isotope ratios and rare earth elements in 3.3 to 4.4 Ga zircons: ion microprobe evidence for high $\delta^{18}\text{O}$ continental crust and oceans in the Early Archaean. *Geochem. Cosmochim. Acta* 65, 4215–4229.
- Piazolo, S., Belousova, E., La Fontaine, A., Corcoran, C., Cairney, J.M., 2017. Trace element homogeneity from micron- to atomic scale: implication for the suitability of the zircon GJ-1 as a trace element reference material. *Chem. Geol.* 456, 10–18.
- Pidgeon, R.T., O'Neil, J.R., Silver, L.T., 1966. Uranium and lead isotopic stability in a metamict zircon under experimental hydrothermal conditions. *Science* 154, 1538–1540.
- Pidgeon, R.T., Nemchin, A.A., Roberts, M.P., Whitehouse, M.J., Bellucci, J.J., 2019. The accumulation of non-formula elements in zircons during weathering: ancient zircons from the Jack Hills, Western Australia. *Chem. Geol.* 530, 119310.
- Rayner, N., Stern, R.A., Carr, S.D., 2005. Grain-scale variations in trace element composition of fluid-altered zircon, Acasta Gneiss Complex, north-western Canada. *Contrib. Mineral. Petrol.* 148, 721–734.
- Robb, L.J., Meyer, F.M., Hawkesworth, C.J., Gardiner, N.J., 2021. Petrogenesis of Archaean granites in the Barberton region of South Africa as a guide to early crustal evolution. *S. Afr. J. Geol.* 124, 111–140.
- Robertson, I.D.M., 1973. Potash granites of the Southern edge of the Rhodesian craton and the northern granulite zone of the Limpopo Mobile Belt. In: LISTER, L.A. (Ed.), *Symposium on Granites, Gneisses and Related Rocks*, vol. 3. Geological Society of South Africa Special Publications, pp. 265–276.
- Rollinson, H.R., 2023. The growth of the Zimbabwe craton during the Neoproterozoic. *Contrib. Mineral. Petrol.* 178, 1. <https://doi.org/10.1007/s00410-022-01978-7>.
- Rollinson, H.R., Blenkinsop, T.G., 1995. The magmatic, metamorphic, and tectonic evolution of the northern marginal zone of the Limpopo belt in Zimbabwe. *Geological Society London* 152, 65–75.
- Rollinson, H., Chagondah, G., Hofmann, A., 2024. The late Archaean granite paradox: a case study from the Zimbabwe Craton, 50th Anniversary Invited Review. *Precamb. Res.* 410, 107491.
- Rollinson, H., Pease, V., 2021. *Using Geochemical Data to Solve Geological Problems*. Cambridge University Press, Cambridge.
- Rollinson, H.R., Whitehouse, M.J., 2011. The growth of the Zimbabwe Craton during the late Archaean: an ion microprobe U-Pb zircon study. *Journal of the Geological Society of London* 168, 941–952.
- Rowe, M.L., Kemp, A.I.S., Wingate, M.T.D., Petersson, A., Whitehouse, M.J., van der Riet, C., 2022. Cratonisation of Archaean continental crust: insights from U-Pb zircon geochronology and geochemistry of granitic rocks in the Narryer Terrane, northwest Yilgarn Craton. *Precamb. Res.* 372, 106609.
- Rubatto, D., 2002. Zircon trace element geochemistry: partitioning with garnet and the link between U-Pb ages and metamorphism. *Chem. Geol.* 184, 123–138.
- Ryerson, F.J., Watson, E.B., 1987. Rutile saturation in magmas: implications for Ti-Nb-Ta depletion in island-arc basalts. *Earth Planet. Sci. Lett.* 86, 225–239.
- Sano, Y., Terada, K., Fukuoka, T., 2002. High mass resolution ion microprobe analysis of rare earth elements in silicate glass, apatite and zircon: lack of matrix dependency. *Chem. Geol.* 184, 217–230.
- Scailliet, B., MacDonald, R., 2001. Phase relations of peralkaline silicic magmas and petrogenetic implications. *J. Petrol.* 42, 825–845.
- Smithies, R.H., Gessner, Y.L.K., Wingate, M.T.D., Champion, D.C., 2018. Geochemistry of Archaean Granitic Rocks in the South West Terrane of the Yilgarn Craton. *Geological Survey of Western Australia. Record* 2018/10.
- Schiller, D., Finger, F., 2019. Application of Ti-in-zircon thermometry to granite studies: problems and possible solutions. *Contrib. Mineral. Petrol.* 174, 1585–1600.
- Storm, L.C., Spear, F.S., 2005. Pressure, temperature and cooling rates of granulite facies migmatitic pelites from the southern Adirondack Highlands, New York. *J. Metamorph. Geol.* 23, 107–130.
- Taylor, P.N., Kramers, J.D., Moorbath, S., Wilson, J.F., Orpen, J.L., Martin, A., 1991. Pb-Pb, Sm-Nd and Rb-Sr geochronology in the Archaean craton of Zimbabwe. *Chem. Geol.* 87, 175–196.
- Taylor, S.R., McLennan, S.M., 1985. *The Continental Crust: its Composition and Evolution*. Oxford, Blackwell.
- Trail, D., Watson, E.B., Tailby, N.D., 2012. Ce and Eu anomalies in zircon as proxies for the oxidation state of magmas. *Geochem. Cosmochim. Acta* 97, 70–87.
- Vervoort, J.D., Kemp, A.I., 2016. Clarifying the zircon Hf isotope record of crust–mantle evolution. *Chem. Geol.* 425, 65–75.
- Watson, E.B., Harrison, T.M., 2005. Zircon thermometer reveals minimum melting conditions on earliest Earth. *Science* 308, 841–844.
- Watson, E., Wark, D., Thomas, J., 2006. Crystallization thermometers for zircon and rutile. *Contrib. Mineral. Petrol.* 151, 413–433.
- Whitehouse, M.J., Kamber, B.S., 2002. On the overabundance of light rare earth elements in terrestrial zircons and its implication for Earth's earliest magmatic differentiation. *Earth Planet. Sci. Lett.* 204, 333–346.
- Wilde, S.A., Valley, J.W., Peck, W.H., Graham, C.M., 2001. Evidence from detrital zircons for the existence of continental crust and oceans on the Earth 4.4 Gyr ago. *Nature* 409, 175–178.
- Wilson, J.F., Nesbitt, R.W., Fanning, C.M., 1995. Zircon geochronology of Archaean felsic sequences in the Zimbabwe craton: a revision of greenstone stratigraphy and a model for crustal growth. In: Coward, P.M., Ries, A.C. (Eds.), *Early Precambrian Processes*, vol. 95. Geological Society of London Special Publications, pp. 109–126.
- Zhang, S.B., Zheng, Y.F., Zhao, Z.F., 2010. Temperature effect over garnet effect on uptake of trace elements in zircon of TTG-like rocks. *Chem. Geol.* 274, 108–125.